



Effects of Retinal Transcription Regulation After GB20 Needling Treatment in Retina With Optic Neuritis

Jie Chen^{1,2†}, Li Zhang^{2†}, Xiulun Gan^{3†}, Rong Zhang², Yinjia He², Qiuyi Lv², Haonan Fu², Xiaodong Liu^{2*} and Linqing Miao^{1,4*}

¹Beijing Advanced Innovation Center for Intelligent Robots and Systems, Beijing Institute of Technology, Beijing, China, ²School of Acupuncture-Moxibustion and Tuina, Beijing University of Chinese Medicine, Beijing, China, ³School of Traditional Chinese Medicine, Beijing University of Chinese Medicine, Beijing, China, ⁴School of Mechatronical Engineering, Beijing Institute of Technology, Beijing, China

OPEN ACCESS

Edited by:

Dumitru A. Iacobas,
Prairie View A&M University,
United States

Reviewed by:

Daniel Adesse,
Oswaldo Cruz Foundation (Fiocruz),
Brazil
Hilda Petrs-Silva,
Federal University of Rio de Janeiro,
Brazil

*Correspondence:

Xiaodong Liu
xiaodongsheldon@outlook.com
Linqing Miao
linqingmiao@gmail.com

[†]These authors share first authorship

Received: 01 June 2020

Accepted: 13 August 2020

Published: 29 September 2020

Citation:

Chen J, Zhang L, Gan X, Zhang R, He Y, Lv Q, Fu H, Liu X and Miao L (2020) Effects of Retinal Transcription Regulation After GB20 Needling Treatment in Retina With Optic Neuritis. *Front. Integr. Neurosci.* 14:568449. doi: 10.3389/fnint.2020.568449

Optic neuritis (ON) is one of the most frequent symptoms of multiple sclerosis (MS) that results in progressive loss of axons and neurons. In clinical trials of Traditional Chinese Medicine, needling at the GB20 acupoint has been widely used for the treatment of ocular diseases, including ON. However, the molecular mechanisms of needling at this site are still unclear. In this study, we generated an experimental autoimmune encephalomyelitis (EAE) mouse model and investigated the effects of needling treatment at the GB20 acupoint on retina with EAE-associated ON. RNA sequencing of the retinal transcriptome revealed that, of the 234 differentially expressed genes induced by ON, 100 genes were upregulated, and 134 genes were downregulated by ON, while needling at the GB20 acupoint specifically reversed the expression of 21 genes compared with control treatment at GV16 acupoint. Among the reversed genes, Nr4a3, Sncg, Uchl1, and Tppp3 were involved in axon development and regeneration and were downregulated by ON, indicating the beneficial effect of needling at GB20. Further gene ontology (GO) enrichment analysis revealed that needling at GB20 affected the molecular process of Circadian rhythm in mouse retina with ON. Our study first reported that needling treatment after ON at the GB20 acupoint regulated gene expression of the retina and reversed the expression of downregulated axon development-related genes. This study also demonstrated that GV16 was a perfect control treatment site for GB20 in animal research. Our study provided a scientific basis for needling treatments at GB20 for ocular diseases.

Keywords: needling, GB20 (Fengchi), GV16 (Fengfu), RNA sequencing, optic neuritis

INTRODUCTION

Multiple sclerosis (MS) is one of the most common inflammatory demyelinating diseases of the central nervous system, characterized by inflammation, demyelination, axonal loss, and gliosis. In MS patients, inflammation predominately affects the white matter of the brain and spinal cord, and it leads to typical presenting syndromes, including monocular visual loss, limb weakness, sensory

loss, double vision, and ataxia, depending on the location of the MS lesions (Lassmann, 2018, 2019; Reich et al., 2018). As a major target in MS, the optic nerve axon could be easily injured, resulting in optic neuritis (ON). ON is a common manifestation and the second most frequent symptom of MS (Kemenyova et al., 2014). It mainly occurs in the setting of MS, and patients with ON typically show a progressive unilateral visual loss of variable severity (de Seze, 2013). The underlying mechanisms of MS-associated ON remain unclear, and there is no satisfactory treatment that could fully prevent visual disability (Woung et al., 2011). In some patients with typical demyelinating ON, no treatment is required, and visual loss is expected to recover from relapses spontaneously (Jenkins and Toosy, 2017). However, most relapses leave behind such persistent damage as color vision, contrast sensitivity, and depth perception abnormalities after the recovery of visual acuity (Dobson and Giovannoni, 2019). Evidence has demonstrated that steroid treatment could accelerate visual recovery but could not improve final visual outcome (Brusaferri and Candelise, 2000). In addition, for patients who fail to recover, no suitable therapy is available.

Needling is a kind of mechanical stimulation and a prevalent clinical methodology based on Traditional Chinese Medicine, which presents great therapeutic effects on ocular diseases without many side-effects. It has been used for treatment of ocular diseases like glaucoma, age-related macular degeneration, retinitis pigmentosa, et cetera (Jiao, 2011; Xu et al., 2012; Law and Li, 2013; Xu and Peng, 2015). According to Traditional Chinese Medicine, treatment sites of GB20 and BL1 acupoint are widely used for ON therapy. GB20 and BL1 were also selected for needling treatment of other ocular diseases (Xu and Peng, 2015; Qin et al., 2015). Our previous study showed that GB20 was more suitable than BL1 in animal study of ocular diseases (Chen et al., 2019). Although the application of needling has shown good clinical efficacy in the treatment of MS-associated ON, the mechanisms of needling are totally unknown. In this study, we use the experimental autoimmune encephalomyelitis (EAE)-optic neuritis (EAE-ON) model to elucidate the scientific basis of needling treatment of ON. EAE is a suitable model, in which animals develop inflammatory-demyelinating diseases spontaneously and cover the specific spectrum of the pathological and immunological features of MS (Lassmann and Bradl, 2017). In mice, the EAE-ON model is induced by injection of myelin oligodendrocyte glycoprotein (MOG) peptide-MOG35–55, and clinical EAE scores are graded daily and blindly according to the standard scoring system (Dietrich et al., 2018; Locri et al., 2018; Torre-Fuentes et al., 2020). Our previous results showed that retinal ganglion cells (RGC), in the retina, were most affected by ON (Huang et al., 2017). We also found that needling at GB20 increased RGC survival in an optic nerve crush model (Chen et al., 2019). However, the effect of needling at GB20 on retina with ON is still unclear. RNA sequencing (RNA-seq) is a new technique effective in identifying numerous genes regulated by specific treatment. Therefore, we take advantage of RNA-seq technique and the EAE mouse model to identify and analyze the differentially expressed retinal genes induced by inflammatory demyelination and the

genes reversed after needling treatment at GB20 and reveal the regulation effects of needling treatment on the retina with ON.

MATERIALS AND METHODS

Animals

We perform experiments on 8-week-old female C57BL/6 mice. All animal procedures were performed in accordance with the National Institute of Health guidelines. The protocol was approved by the Animal Care and Use Committee of Beijing Institute of Technology and Peking University.

MOG Immunization and EAE Model Preparation

Female 8-week-old C57BL/6 mice were immunized with 150 μ g MOG35–55 peptide emulsified with complete Freund's adjuvant (CFA) and 2.5 mg/ml mycobacterium tuberculosis, followed by immunization of 200 ng pertussis toxin at day 0 and day 2 (Quinn et al., 2011). The behavioral deficits of these mice were assessed daily with a 5-point scale (Gran et al., 2002), as follows: limp tail, 1; limp tail with waddling gait, 1.5; partial limb paralysis, 2; full paralysis of one limb, 2.5; full paralysis of one limb with partial paralysis of second limb, 3; full paralysis of two limbs, 3.5; moribund, 4; and death, 5. The clinical score was recorded every other day until 5 weeks post-immunization.

Needling Treatment

Three weeks after MOG immunization, mice were anesthetized by xylazine and ketamine based on their body weight (0.01 mg xylazine/g + 0.08 mg ketamine/g) before needling treatment at acupoint GB20 or GV16 at both sides, respectively. The depth of the needling is around 2 mm. The duration of needling treatment was 20 min. EAE mice were treated with needling treatments 3 weeks after MOG immunization and treated every 3 days for 2 weeks before sacrifice.

RNA Preparation

Mice were randomly divided into four groups (two or three mice/group). Experiments were repeated for three times. Briefly, in each replicate, mice were sacrificed 5 weeks after MOG immunization, and retinas were dissected out in HBSS buffer (Cellgro) immediately. Retinas were then homogenized with TRIzol Reagent (Thermo Fisher Scientific), and total RNA was extracted from the homogenized mixture according to the reagent instructions. RNA purity was checked using the NanoPhotometer[®] spectrophotometer (IMPLEN). RNA concentration was measured using Qubit[®] RNA Assay Kit in Qubit[®] 2.0 Fluorometer (Life Technologies). RNA integrity was assessed using the RNA Nano 6000 Assay Kit of the Bioanalyzer 2100 system (Agilent Technologies).

Library Preparation and Sequencing

About 5 μ g total RNA generated from each group was used for RNA-seq, which was done at Novogene, Inc. Briefly, RNA samples from three biological replicates went through mRNA purification with poly-T oligo-attached magnetic

beads. Sequencing libraries were generated using NEBNext[®] Ultra[™] RNA Library Prep Kit for Illumina[®] (NEB) following manufacturer's recommendations and index codes were added to attribute sequences to each sample. The library fragments were purified with the AMPure XP system (Beckman Coulter) for cDNA fragments of preferentially 250–300 bp in length. Library quality was assessed on the Agilent Bioanalyzer 2100 system. The clustering of the index-coded samples was performed on a cBot Cluster Generation System using TruSeq PE Cluster Kit v3-cBot-HS (Illumina) according to the manufacturer's instructions. After cluster generation, the library preparations were sequenced on an Illumina HiSeq platform and 125/150 bp paired-end reads were generated.

Gene Expression Analysis

The RNA-seq reads were aligned to the reference genome using Hisat2 v2.0.5. FeatureCounts v1.5.0-p3 was used to count the reads numbers mapped to each gene. We used Fragments Per Kilobase of transcript sequence per Millions base pairs sequenced (FPKM) to represent relative gene expression abundance. FPKM of each gene was calculated based on the length of the gene and reads count mapped to this gene, which normalizes gene expression by considering the effect of sequencing depth and gene transcript length at the same time. Differential expression analysis was performed using the DESeq2 R package (1.16.1). The resulting *p*-values were adjusted using the Benjamini and Hochberg's approach for controlling the false discovery rate (less than 0.05). Genes with an adjusted *p*-value (*padj*) < 0.05 (detected by DESeq2) were considered differentially expressed.

Statistical Analysis

An adjusted *p*-value < 0.05 was considered as statistically significant. The raw data and GEO accession number for this study are as follows: GSE148759, link: <https://www.ncbi.nlm.nih.gov/geo/query/acc.cgi?acc=GSE148759>.

RESULTS

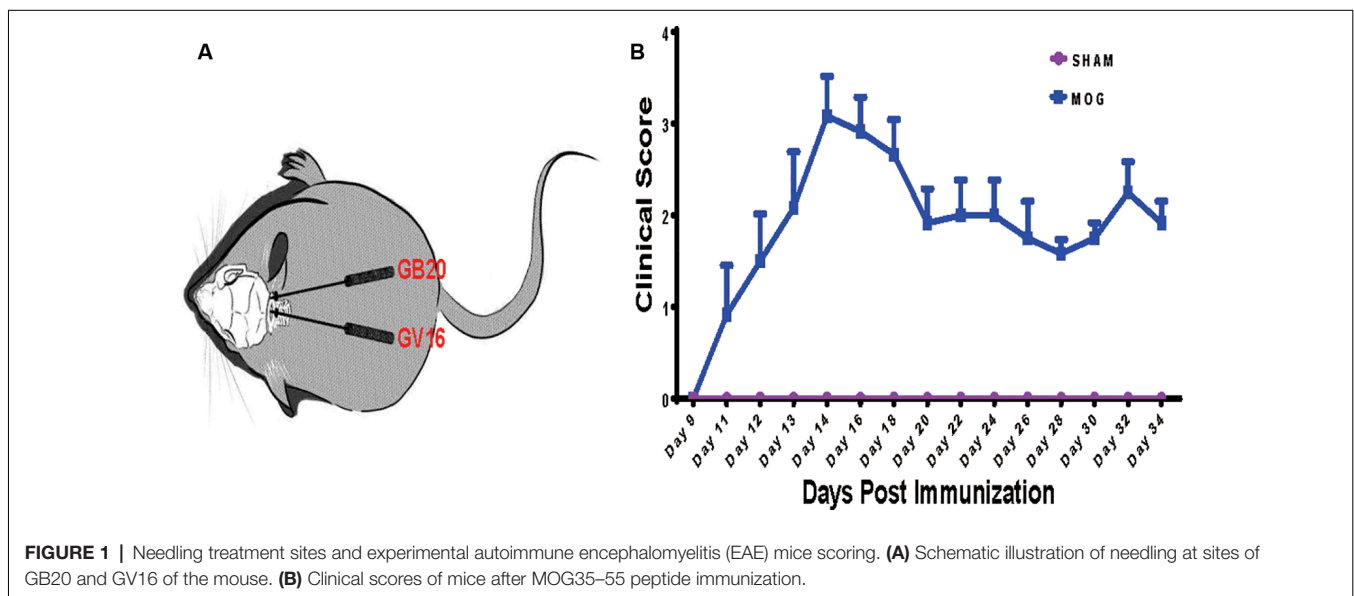
Expression Analysis

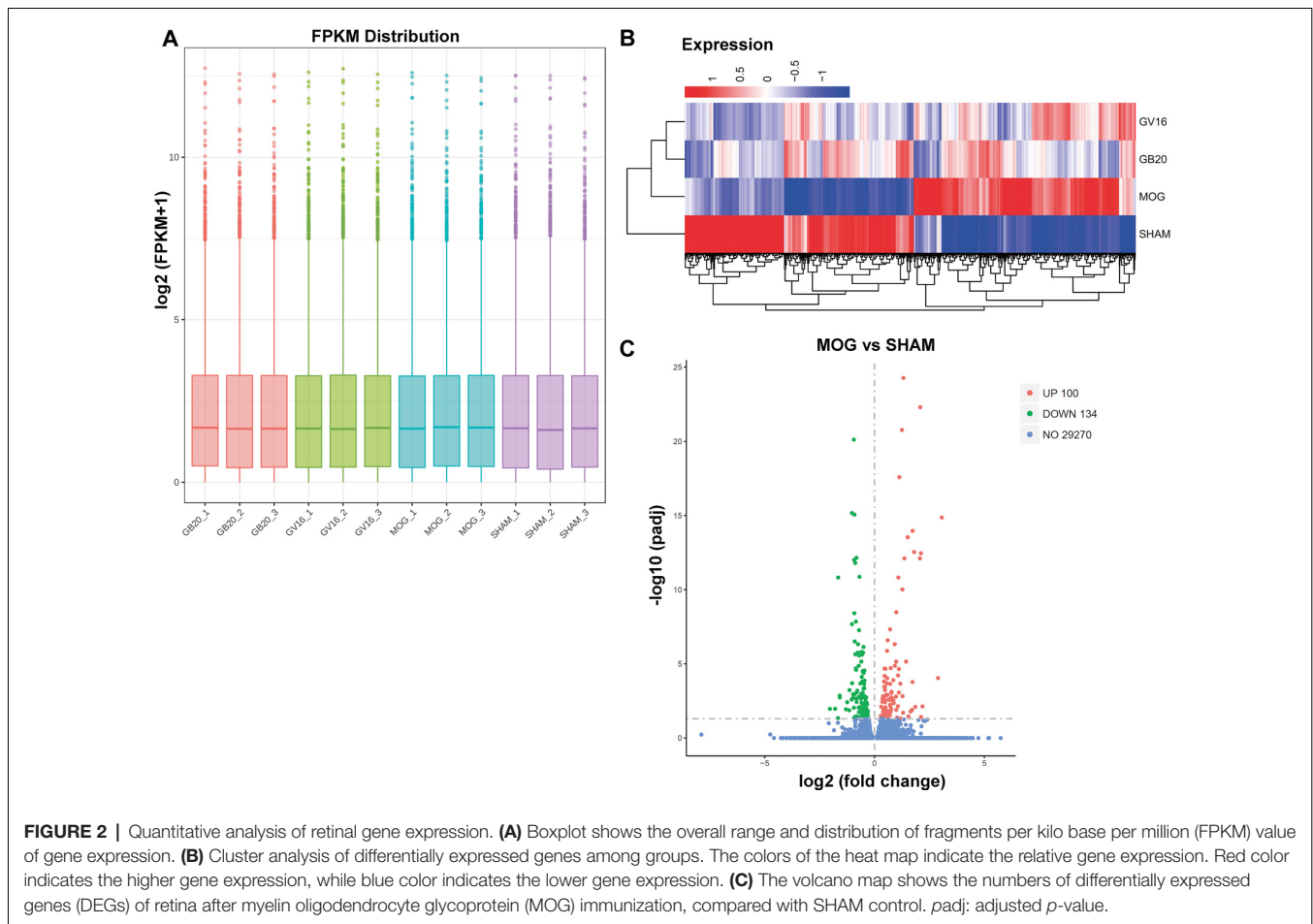
To investigate the effects of needling treatments on regulation of retinal gene expression in EAE/ON models, we extracted retinal RNA 5 weeks after immunization, from SHAM control group (SHAM), MOG immunization group (MOG) and MOG immunization mice with needling treatments at acupoint GB20 (GB20) or control acupoint GV16 (GV16). The schematic image illustrated the needling treatment sites of GB20 and GV16 (Figure 1A). Scores on a five-point scale showed the clinical development of mice after MOG immunization (Figure 1B). Needling treatment at GB20 or GV16 did not affect the EAE clinical score (data not shown).

RNA integrity of each sample was assessed by Bioanalyzer 2100 system. Sample total reads ranged from 44.4 to 54.7 million, and the mapping rate of sample total reads to mouse reference genome ranged from 97.0 to 97.3%. We used FPKM to represent relative gene expression abundance. The boxplot result showed that the overall distribution of the FPKM values were consistent among samples, suggesting that the RNA-seq data were reproducible (Figure 2A). Cluster analysis showed that needling treatment groups were clustered together and separated from MOG control, and all the MOG groups with or without needling treatments were separated from SHAM control group (Figure 2B).

Differentially Expressed Retinal Genes by MOG Immunization

To identify candidate genes affected by optic neuritis, we performed differential expression analysis using the DESeq2 R package (1.16.1). Genes with $|\log_2\text{FoldChange}| > 0$ and an adjusted *p*-value < 0.05 were assigned as differentially expressed. We then identified 234 differentially expressed genes (DEGs) in total, with 100 genes upregulated and 134 genes down-regulated (Figure 2C). The top most upregulated gene,





Ecell, had an alternative name “damage-induced neuronal endopeptidase,” whose molecular functions were metal ion binding and metalloendopeptidase activity (Kiryu-Seo et al., 2000). Ecell was increased by eight times after ON and the *p*-value was 1.41×10^{-15} , which was incredibly significant. The second most upregulated gene, Oas2, was an interferon-induced dsRNA-activated antiviral enzyme that played a critical role in cellular innate antiviral response (Oakes et al., 2017). It also played a role in other cellular processes such as apoptosis, cell growth, differentiation and gene regulation (Kristiansen et al., 2011). Oas2 was increased by seven times after ON and the *p*-value was 9.17×10^{-5} . The third most up-regulated gene was unknown. The fourth most upregulated gene, Cxcl10, was a pro-inflammatory cytokine that was involved in processes such as activation of peripheral immune cells, regulation of cell growth, apoptosis and modulation of angiostatic effects (Gao et al., 2017). Activation of the CXCL10/CXCR3 axis also played an important role in neurons in response to brain injury (Rappert et al., 2004). Cxcl10 was increased by four times after ON and the *p*-value was 0.0389. The fifth most upregulated gene, Tnnt2, whose molecular functions were actin binding and calcium ion binding, was increased by four times after ON and the *p*-value was 3.61×10^{-13} . The top most down-regulated gene, Ppp1r1c, was a protein phosphatase inhibitor, increasing cell susceptibility

to TNF-induced apoptosis. Ppp1r1c was down-regulated by 75% after ON and the *p*-value was 0.0107. The second most down-regulated gene, Oxtr, was a G-protein coupled receptor involved in many biological processes such as positive regulation of synapse assembly and synaptic transmission. Oxtr was down-regulated by 71% after ON and the *p*-value was 0.011. The third most down-regulated gene, Egr4, was a transcriptional regulator, activating the transcription of target genes required for mitogenesis and differentiation. Egr4 was down-regulated by 68% after ON and the *p*-value was 4.49×10^{-2} . The fourth most down-regulated gene, Scn4b, was a voltage-gated sodium channel subunit, positively regulating sodium ion transport. Scn4b was down-regulated by 68% after ON and the *p*-value was 1.57×10^{-11} . The fifth most down-regulated gene was an unknown gene. The top 20 upregulated and down-regulated DEGs together with the information of log2 FoldChange and *p*-value were listed in **Table 1**. Among the 20 down-regulated DEGs, there were four transcription factors, Egr4, Nr4a3, Isl2, and Pou4f1, which were highlighted in yellow (**Table 1**). The transcription factor Nr4a3 functioned in negative regulation of apoptotic process, and was reported to play a neuroprotection role in oxidative stress-induced neuron death (Rappert et al., 2004). Nr4a3 was down-regulated by 67% after ON and the *p*-value was 0.00183. The transcription factor Isl2, was reported to be involved in

TABLE 1 | Top 20 upregulated and 20 down-regulated retinal genes induced by optic neuritis (ON).

gene_name	log2FoldChange	p value	gene_id	gene_description
Up-regulated DEG				
Ecel1	3.062	1.41E-15	ENSMUSG00000026247	endothelin converting enzyme-like 1 [Source:MGI Symbol;Acc:MGI:1343461]
Oas2	2.892	9.17E-05	ENSMUSG00000032690	2'-5' oligoadenylate synthetase 2 [Source:MGI Symbol;Acc:MGI:2180852]
E230001N04Rik	2.186	7.48E-03	ENSMUSG00000066170	RIKEN cDNA E230001N04 gene [Source:MGI Symbol;Acc:MGI:2443549]
Cxcl10	2.121	3.89E-02	ENSMUSG00000034855	chemokine (C-X-C motif) ligand 10 [Source:MGI Symbol;Acc:MGI:1352450]
Tnnt2	2.114	3.61E-13	ENSMUSG00000026414	troponin T2, cardiac [Source:MGI Symbol;Acc:MGI:104597]
Serpina3n	2.083	5.30E-23	ENSMUSG00000021091	serine (or cysteine) peptidase inhibitor, clade A, member 3N [Source:MGI Symbol;Acc:MGI:105045]
Lad1	2.068	7.99E-13	ENSMUSG00000041782	ladinin [Source:MGI Symbol;Acc:MGI:109343]
Calca	1.859	7.95E-03	ENSMUSG00000030669	calcitonin/calcitonin-related polypeptide, alpha [Source:MGI Symbol;Acc:MGI:2151253]
Gpnmb	1.803	3.00E-13	ENSMUSG00000029816	glycoprotein (transmembrane) nmb [Source:MGI Symbol;Acc:MGI:1934765]
C4b	1.732	1.10E-14	ENSMUSG00000073418	complement component 4B (Chido blood group) [Source:MGI Symbol;Acc:MGI:88228]
Edn2	1.732	1.68E-04	ENSMUSG00000028635	endothelin 2 [Source:MGI Symbol;Acc:MGI:95284]
Bcl3	1.711	1.26E-02	ENSMUSG00000053175	B cell leukemia/lymphoma 3 [Source:MGI Symbol;Acc:MGI:88140]
Rpe65	1.644	1.62E-02	ENSMUSG00000028174	retinal pigment epithelium 65 [Source:MGI Symbol;Acc:MGI:98001]
Nlrc5	1.540	3.52E-02	ENSMUSG00000074151	NLR family, CARD domain containing 5 [Source:MGI Symbol;Acc:MGI:3612191]
A2m	1.514	2.99E-14	ENSMUSG00000030111	alpha-2-macroglobulin [Source:MGI Symbol;Acc:MGI:2449119]
Gbp2	1.440	7.09E-06	ENSMUSG00000028270	guanylate binding protein 2 [Source:MGI Symbol;Acc:MGI:102772]
Osmr	1.358	7.98E-13	ENSMUSG00000022146	oncostatin M receptor [Source:MGI Symbol;Acc:MGI:1330819]
BC055402	1.311	5.65E-25	ENSMUSG00000010429	cDNA sequence BC055402 [Source:MGI Symbol;Acc:MGI:3039597]
Gm48237	1.301	1.96E-02	ENSMUSG000000113580	predicted gene, 48237 [Source:MGI Symbol;Acc:MGI:6097646]
Fbn2	1.274	1.52E-03	ENSMUSG00000024598	fibrillin 2 [Source:MGI Symbol;Acc:MGI:95490]
Down-regulated DEG				
Ppp1r1c	-2.027	1.07E-02	ENSMUSG00000034683	protein phosphatase 1, regulatory inhibitor subunit 1C [Source:MGI Symbol;Acc:MGI:1923185]
Oxtr	-1.794	1.10E-02	ENSMUSG00000049112	oxytocin receptor [Source:MGI Symbol;Acc:MGI:109147]
Egr4	-1.660	4.49E-02	ENSMUSG00000071341	early growth response 4 [Source:MGI Symbol;Acc:MGI:99252]
Scn4b	-1.656	1.57E-11	ENSMUSG00000046480	sodium channel, type IV, beta [Source:MGI Symbol;Acc:MGI:2687406]
Gm8325	-1.584	1.40E-03	ENSMUSG00000027694	predicted pseudogene 8325 [Source:MGI Symbol;Acc:MGI:3644852]
Nr4a3	-1.582	1.83E-03	ENSMUSG00000028341	nuclear receptor subfamily 4, group A, member 3 [Source:MGI Symbol;Acc:MGI:1352457]
Sh3bgr	-1.302	1.15E-02	ENSMUSG00000040666	SH3-binding domain glutamic acid-rich protein [Source:MGI Symbol;Acc:MGI:1354740]
Prph	-1.240	3.90E-03	ENSMUSG00000023484	peripherin [Source:MGI Symbol;Acc:MGI:97774]
Gm9866	-1.151	1.35E-02	ENSMUSG00000094002	predicted gene 9866 [Source:MGI Symbol;Acc:MGI:3643118]
Isl2	-1.141	5.94E-04	ENSMUSG00000032318	insulin related protein 2 (islet 2) [Source:MGI Symbol;Acc:MGI:109156]
Coro6	-1.040	2.51E-03	ENSMUSG00000020836	coronin 6 [Source:MGI Symbol;Acc:MGI:2183448]
Pou4f1	-1.026	2.16E-08	ENSMUSG00000048349	POU domain, class 4, transcription factor 1 [Source:MGI Symbol;Acc:MGI:102525]
Nefm	-1.026	6.71E-16	ENSMUSG00000022054	neurofilament, medium polypeptide [Source:MGI Symbol;Acc:MGI:97314]
Pvalb	-1.021	2.04E-04	ENSMUSG00000005716	parvalbumin [Source:MGI Symbol;Acc:MGI:97821]
Ctxn3	-0.976	1.14E-03	ENSMUSG00000069372	cortixin 3 [Source:MGI Symbol;Acc:MGI:3642816]
Fxyd7	-0.971	1.91E-03	ENSMUSG00000036578	FXD domain-containing ion transport regulator 7 [Source:MGI Symbol;Acc:MGI:1889006]
Nefl	-0.938	7.16E-21	ENSMUSG00000022055	neurofilament, light polypeptide [Source:MGI Symbol;Acc:MGI:97313]
Hipk4	-0.934	9.08E-03	ENSMUSG00000040424	homeodomain interacting protein kinase 4 [Source:MGI Symbol;Acc:MGI:2685008]
Sncg	-0.931	9.99E-13	ENSMUSG00000023064	synuclein, gamma [Source:MGI Symbol;Acc:MGI:1298397]
Nrn1	-0.923	3.92E-09	ENSMUSG00000039114	neuritin 1 [Source:MGI Symbol;Acc:MGI:1915654]

Genes were selected by adjusted *p*-value (*padj*) < 0.05, $|\log_2\text{FoldChange}| > 0$ and *FPKM* > 0, genes highlighted in yellow are transcription factors.

axonogenesis and retinal ganglion cell axon guidance (Pak et al., 2004). *Isl2* was down-regulated by 55% after ON, and the *p*-value was 0.000594. The transcription factor *Pou4f1*, also named *Brn3a*, was another negative regulator of apoptotic process (Hudson et al., 2008; Dykes et al., 2010). *Pou4f1* was down-regulated by 51% after ON and the *p*-value was 2.16×10^{-8} .

Enrichment Analysis of DEGs Induced by Optic Neuritis

To analyze the overall regulation effects of these DEGs induced by ON, we performed enriched gene ontology (GO) analysis. Results showed that among the three main categories of Biological Process (BP), Cellular Component (CC), and Molecular Function (MF), the top three most significantly regulated gene categories were: neurofilament, axonogenesis and axon development (Figure 3A). Axonogenesis and axon development were belonged to the main category of BP, while neurofilament was belonged to the main category of CC. As to

the top 3 GeneRatio categories which contained the most count of DEGs, they were axonogenesis, axon development and axon part (Figure 3B). Axon parts also belonged to the main category of CC. However, enriched KEGG (Kyoto Encyclopedia of Genes and Genomes) pathway analysis showed no significant enriched gene categories (Supplementary Figure S1).

Reversal of Optic Neuritis Induced DEGs by Needling Treatment

To study the effect of needling treatment in mice with ON, we performed needling treatments every 3 days at acupoint GB20 or control acupoint GV16 3 weeks after MOG immunization. RNA-seq analysis showed that among the ON induced 234 DEGs, GB20 treatment significantly upregulated 13 and down-regulated 24 of total DEGs (Figure 4A), while GV16 control treatment significantly up-regulated 4 and down-regulated 14 of total DEGs (Figure 4B). Further analysis revealed that, of the ON induced 100 up-regulated DEGs (MOG

TABLE 2 | Differentially expressed genes (DEGs) reversed by needling treatments.

Reverse of up-regulated DEGs			
Gene ID	Gene_name	Gene_description	MOG vs. SHAM log2FoldChange
ENSMUSG00000029816	Gprmb	glycoprotein (transmembrane) nmb [Source:MGI Symbol:Acc:MGI:1934765]	1.80
ENSMUSG00000036480	Prss56	protease, serine 56 [Source:MGI Symbol:Acc:MGI:1916703]	1.27
ENSMUSG00000020080	Hkdc1	hexokinase domain containing 1 [Source:MGI Symbol:Acc:MGI:2384910]	1.08
ENSMUSG00000024598	Fbn2	fibillin 2 [Source:MGI Symbol:Acc:MGI:95490]	1.27
ENSMUSG00000023868	Pde10a	phosphodiesterase 10A [Source:MGI Symbol:Acc:MGI:1345143]	1.06
ENSMUSG00000031538	Plat	plasminogen activator, tissue [Source:MGI Symbol:Acc:MGI:97610]	0.92
ENSMUSG0000000957	Mmp14	matrix metalloproteinase 14 (membrane-inserted) [Source:MGI Symbol:Acc:MGI:101900]	0.71
ENSMUSG00000101429	BC055402	cDNA sequence BC055402 [Source:MGI Symbol:Acc:MGI:3039597]	1.31
ENSMUSG00000114414	A930014D07Rik	RIKEN cDNA A930014D07 gene [Source:MGI Symbol:Acc:MGI:1925197]	0.77
ENSMUSG00000021446	Osmr	oncostatin M receptor [Source:MGI Symbol:Acc:MGI:1330819]	1.36
ENSMUSG00000031502	Col4a1	collagen, type IV, alpha 1 [Source:MGI Symbol:Acc:MGI:88454]	0.53
ENSMUSG00000006782	Cnp	2',3'-cyclic nucleotide 3' phosphodiesterase [Source:MGI Symbol:Acc:MGI:88437]	0.50
ENSMUSG00000041479	Syt15	synaptotagmin XV [Source:MGI Symbol:Acc:MGI:2442166]	0.50
ENSMUSG000000056752	Dnah9	dynein, axonemal, heavy chain 9 [Source:MGI Symbol:Acc:MGI:1289279]	0.53
ENSMUSG00000037656	Slc20a2	solute carrier family 20, member 2 [Source:MGI Symbol:Acc:MGI:97851]	0.47
ENSMUSG00000030905	Crym	crystallin, mu [Source:MGI Symbol:Acc:MGI:102675]	0.60
ENSMUSG00000021071	Trim9	tripartite motif-containing 9 [Source:MGI Symbol:Acc:MGI:2137354]	0.50
ENSMUSG00000063142	Kcnma1	potassium large conductance calcium-activated channel, subfamily M, alpha member 1 [Source:MGI Symbol:Acc:MGI:99923]	0.33
ENSMUSG00000022912	Prosl	protein 5 (alpha) [Source:MGI Symbol:Acc:MGI:1095733]	0.66
ENSMUSG00000024411	Aqp4	aquaporin 4 [Source:MGI Symbol:Acc:MGI:107387]	0.46
ENSMUSG00000022272	Myo10	myosin X [Source:MGI Symbol:Acc:MGI:107716]	0.48
ENSMUSG000000051000	Fam160a1	family with sequence similarity 160, member A1 [Source:MGI Symbol:Acc:MGI:2444746]	0.30
ENSMUSG00000075254	Heg1	heart development protein with EGF-like domains 1 [Source:MGI Symbol:Acc:MGI:1924696]	0.37
ENSMUSG00000022797	Tfrc	transferrin receptor [Source:MGI Symbol:Acc:MGI:98822]	0.28
Reverse of down-regulated DEGs			
ENSMUSG00000028341	Nr4a3	nuclear receptor subfamily 4, group A, member 3 [Source:MGI Symbol:Acc:MGI:1352457]	-1.58
ENSMUSG00000038560	Ciart	circadian associated repressor of transcription [Source:MGI Symbol:Acc:MGI:2684975]	-0.85
ENSMUSG00000062563	Cys1	cystin 1 [Source:MGI Symbol:Acc:MGI:2177632]	-0.70
ENSMUSG00000020062	Slc5a8	solute carrier family 5 (iodide transporter), member 8 [Source:MGI Symbol:Acc:MGI:2384916]	-0.72
ENSMUSG00000059824	Dbp	D site albumin promoter binding protein [Source:MGI Symbol:Acc:MGI:94866]	-0.50
ENSMUSG00000023064	Sncg	synuclein, gamma [Source:MGI Symbol:Acc:MGI:1298397]	-0.93
ENSMUSG00000031431	Tsc22d3	TSC22 domain family, member 3 [Source:MGI Symbol:Acc:MGI:1196284]	-0.40
ENSMUSG00000014846	Tppp3	tubulin polymerization-promoting protein family member 3 [Source:MGI Symbol:Acc:MGI:1915221]	-0.85
ENSMUSG00000021102	Glxr5	glutaredoxin 5 [Source:MGI Symbol:Acc:MGI:1920296]	-0.51
ENSMUSG00000030103	Bhlhe40	basic helix-loop-helix family, member e40 [Source:MGI Symbol:Acc:MGI:1097714]	-0.35
ENSMUSG00000029223	Uchl1	ubiquitin carboxy-terminal hydrolase L1 [Source:MGI Symbol:Acc:MGI:103149]	-0.83
ENSMUSG00000021991	Cacna2d3	calcium channel, voltage-dependent, alpha2/delta subunit 3 [Source:MGI Symbol:Acc:MGI:1338890]	-0.39

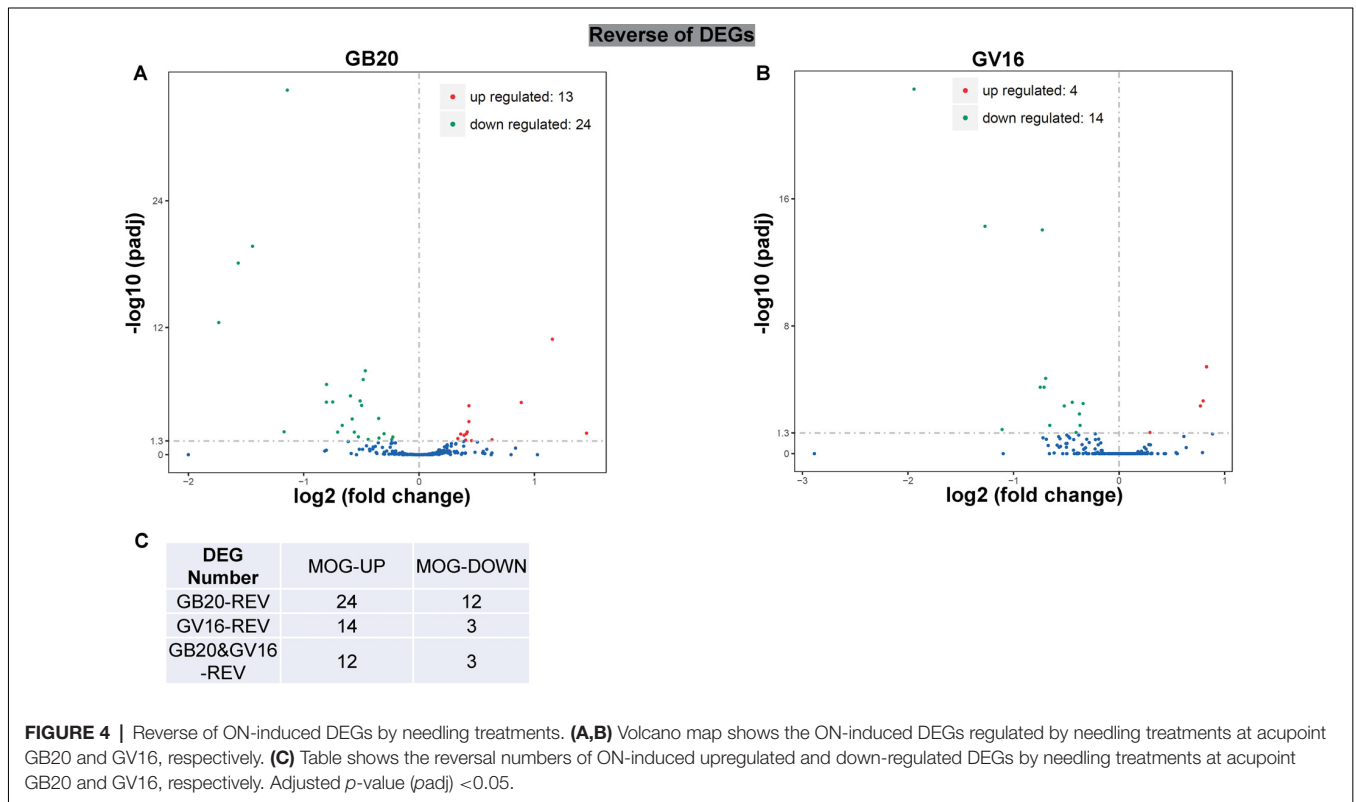
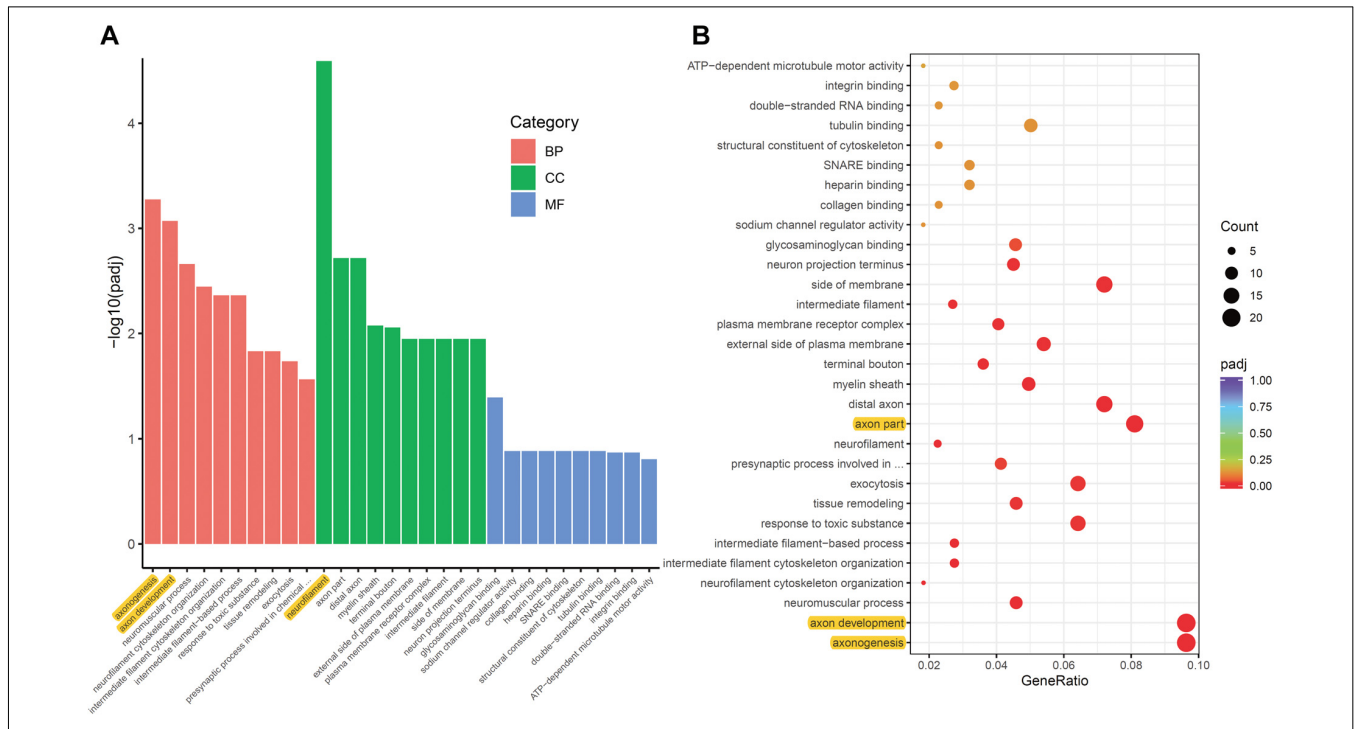
Reversed DEGs were selected by adjusted *p*-value (*padj*) < 0.05, |log₂FoldChange| > 0 and FPKM > 0. The green color highlights the DEGs specifically reversed by needling treatment at GB20, while yellow highlights the DEGs reversed both by needling treatment at GB20 and GV16.

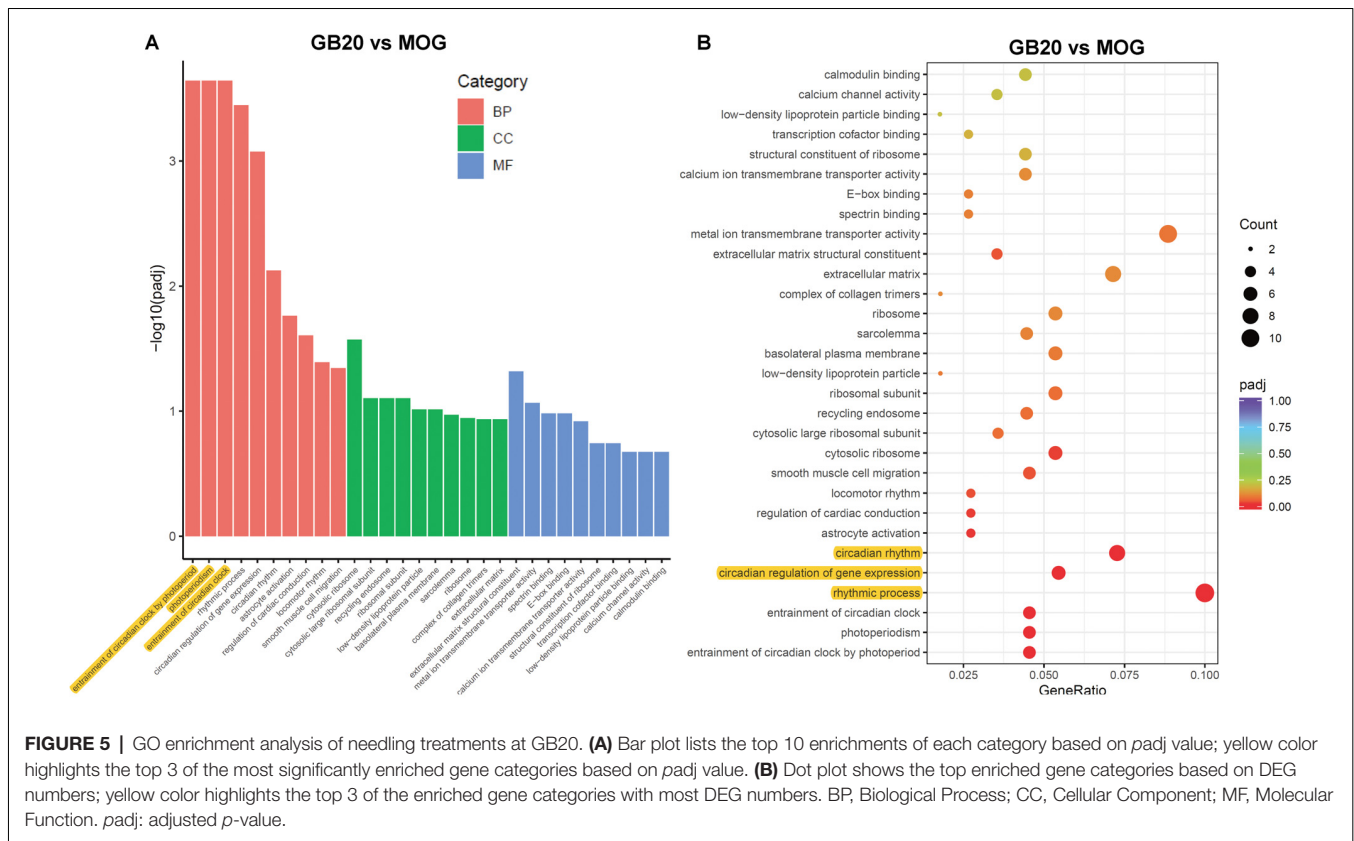
vs. SHAM), 24 DEGs were reversed by GB20 treatment, while 14 were reversed by control GV16 treatment. However, 12 of the 14 reversed DEGs of GV16 treatment were already included in the 24 DEGs of GB20 (Figure 4C). The left 2 DEGs specific to GV16 control were Gfap (glial fibrillary acidic protein) and Fgf2 (fibroblast growth factor 2). Therefore, after deducting the same DEGs shared by GV16 control, there were 12 DEGs specifically down-regulated by GB20. Among the ON induced 134 down-regulated DEGs (MOG vs. SHAM), 12 DEGs were reversed by GB20 treatment, while only three DEGs were reversed by control GV16 treatment, and all the three reversed DEGs of GV16 were also shown in that of GB20, not specific to GV16 treatment (Figure 4C). After deducting the same DEGs shared by GV16 control, there were nine DEGs specifically upregulated by GB20. Together, there were totally 21 DEGs specifically reversed by GB20 treatment compared with control treatment. The reversed DEGs were listed in Table 2. DEGs specifically reversed by GB20 treatment were highlighted in green and DEGs both reversed by GB20 or GV16 treatment were highlighted in yellow (Table 2). Finally, there was one gene whose expression was further enhanced by either GB20 or GV16 treatment, which was Folh1 (folate hydrolase 1). The average FPKM values of the 234 DEGs of all groups were listed in the supplemental data (Supplementary Table S1).

Mechanical stimulation at GB20 acupoint of EAE mice for 2 weeks, was resulted in reverse of total 36 ON induced DEGs (Figure 4C). Specifically, among those reversed DEGs (Table 2), Nr4a3, Sncg and Uchl1 were axonogenesis and axon development related (Soto et al., 2008; Stevanato and Sinden, 2014; Bishop et al., 2016) and down-regulated in EAE model. Tppp3 was involved in tubulin polymerization and promotion of axon regeneration (Huang et al., 2017); and Slc5a8 was involved in sodium ion transmembrane transport (Miyachi et al., 2004). Furthermore, Nr4a3 and Sncg were among the top 20 down-regulated DEGs induced by MOG immunization (Table 1).

Enrichment Analysis of Needling Treatment

To analyze the overall effects of needling treatments on mice with ON, we performed enriched GO analysis comparing GB20 vs. MOG and GV16 vs. MOG. Results showed that the top 3 most significantly regulated gene categories after needling treatment at GB20 were: entrainment of circadian clock by photoperiod, Photoperiodism and Entrainment of circadian clock (Figure 5A). As to the top 3 GeneRatio categories which contained the most count of DEGs, they were Rhythmic process, Circadian rhythm, and Circadian regulation of gene expression (Figure 5B). They were all belonged to main category of BP. However, needling





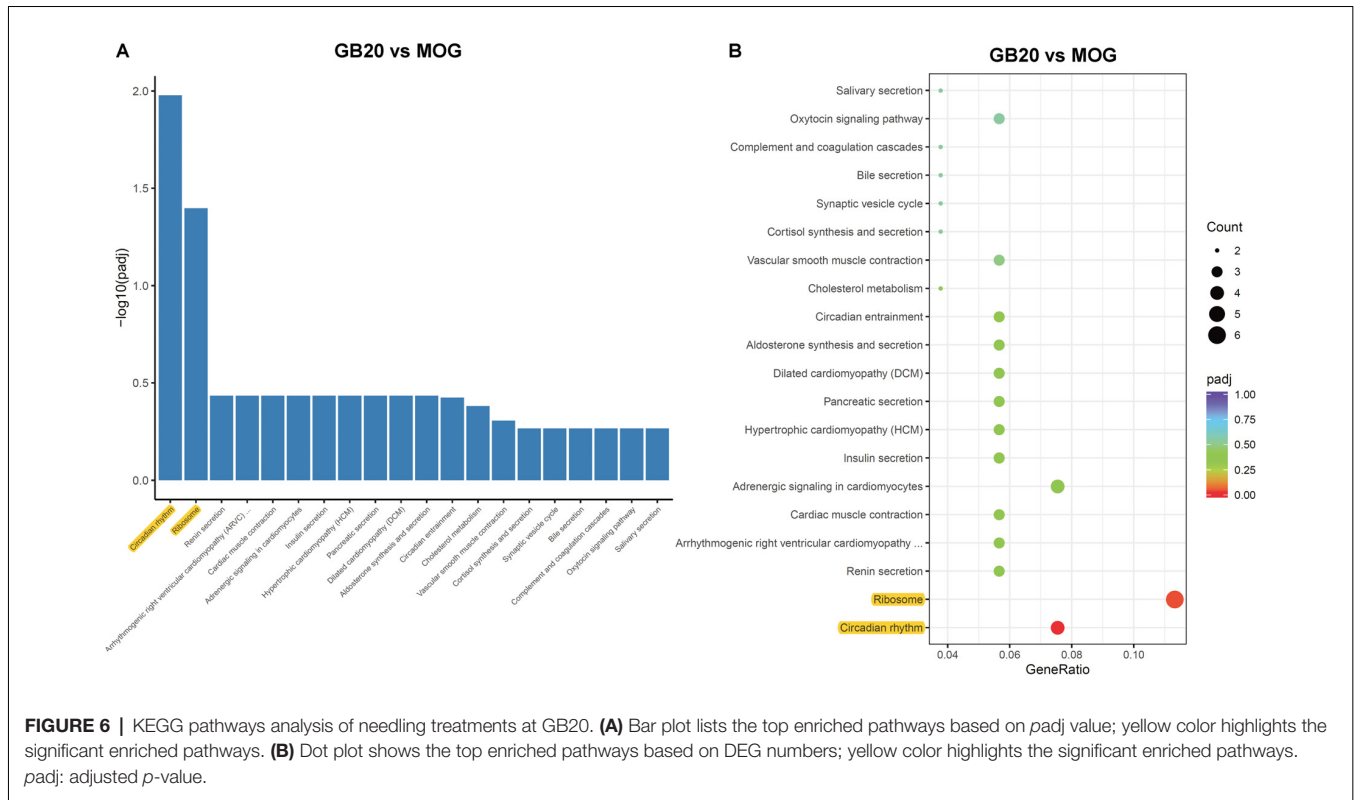
treatment at control acupoint GV16 showed no significant gene category enrichment (**Supplementary Figure S2**). Finally, KEGG pathway enrichment analysis showed that only gene categories of Circadian rhythm and Ribosome were significantly regulated (**Figure 6**). There were a total of 119 DEGs after needling treatment at acupoint GB20 compared with MOG group, while there were only 57 DEGs after needling treatment at control acupoint GV16 compared with MOG group (**Supplementary Figure S3**). The average FPKM values of the 119 DEGs induced by GB20 treatment and 57 DEGs induced by GV16 control treatment were listed in the supplemental tables (**Supplementary Tables S2, S3**).

DISCUSSION

ON is the second most frequent symptom of MS, while there is no satisfactory treatment that could prevent visual disability. In Traditional Chinese Medicine, needling is widely used in clinical trials of ocular disease treatment. However, the underlying mechanism remains unclear. In the present study, by using an EAE mouse model and retinal RNA sequencing, we demonstrate that GB20 needling can regulate the retinal transcriptome of EAE mice and reverse the expression of genes induced by ON. Many studies revealed that endoplasmic reticulum (ER) stress ER stress is closely linked to neuroinflammation. Many key molecules of unfolded protein response (UPR) pathways, such as CHOP, ATF4, BiP, and XBP1, are reported to be induced

in autopsied brain specimens of MS patients and spinal cord of EAE mice (Deslauriers et al., 2011). These ER stress molecules are also induced in retina of EAE mouse (Stone and Lin, 2015; Huang et al., 2017). However, the induction of those key UPR pathway molecules is not found in the RNA sequencing analysis of EAE retina samples. This may be due to the low induction and expression level of ER stress molecules in retina with ON. In our previous study, CHOP, PERK and ATF4 were all induced in optic nerve crush model and identified by RNA sequencing analysis (Chen et al., 2019). Optic neuropathies caused by either traumatic injury such as optic nerve crush and ischemia or chronic injury such as ON all results in retinal degeneration and RGC death (Fernandes et al., 2013; Nashine et al., 2014; Huang et al., 2017; Kumar et al., 2019). Although inhibition of ER stress molecules provides neuroprotection, the manipulation of ER stress molecules does not affect the disease development of EAE mouse (Deslauriers et al., 2011; Huang et al., 2017; Yue et al., 2019). In this study, needling at GB20 specifically reversed the expression of 21 genes induced by ON, while as the same, needling treatment did not affect the clinical score of EAE development.

Among the DEGs reversed by GB20 needling treatment, we found that Nr4a3 is a transcription factor and significantly down-regulated by ON. Nr4a3 plays a critical role in pyramidal cell survival and axonal guidance (Pönniö and Conneely, 2004). Nr4a3 functions as a negative regulator of apoptotic process, and plays a neuroprotection role in oxidative stress-induced neuron death (Volakakis et al., 2010). Needling treatment at



GB20 significantly increased and recovered the expression level of *Nr4a3* (Table 2), indicating that mechanical stimulation at GB20 did have beneficial effects in treatment of ON.

In the previous study, we used GV16 acupoint for the first time as a control needling site for GB20 which was physically very close to the GB20 acupoint (Chen et al., 2019). In the present study, we have again proved that GV16 is the best control site for the needling treatment at GB20. Almost all the DEGs reversed by control GV16 treatment was also shown in the reversed DEG list of GB20 treatment. There are 21 DEGs that are specifically reversed by GB20 treatment (Figure 4C).

The GO enrichment analysis revealed that the most affected gene category of retina was circadian rhythm after treatment at GB20 (Figure 5B). So far, there is no report about the link between the stimulation at GB20 and the regulation of retinal circadian rhythm. Therefore, we are the first to report the connection of GB20 needling to retinal circadian rhythm regulation. There are some studies reported that acupuncture treatment with acupoints combination can upregulate the expression of circadian rhythm genes of *Clock* and *Bmal1* in the hypothalamus (Wei et al., 2017) and the circadian rhythm genes of *Per1* and *Per2* in the suprachiasmatic nucleus (SCN) in insomnia rats (Guo et al., 2017), while some other research group reported that electroacupuncture treatment down-regulated the expression of *Per1* and *Per2* in the SCN (Hou et al., 2018). It is also reported that acupuncture treatments affect the circadian rhythm of blood pressure (Kim et al., 2012; Yang et al., 2016; Lei et al., 2017). Among the above reports, the acupoint GB20 is not included in their acupoint combinations. In this study, single

needling treatment at GB20 also upregulated the gene expression of *Per1* and *Per2* in mouse retina, in accordance with other research groups' reports that acupuncture treatments can affect expression of circadian rhythm genes.

The mechanism of needling at GB20 affects the regulation of retinal gene expression, is still unclear and may be extraordinarily complex, since the site of GB20 is at the back of the neck, far from the eyes (Figure 1A). A previous functional magnetic resonance imaging study revealed that needling at GB20 was able to regulate neural activity within the visual region of the brain (Li et al., 2018). It is reported that needling treatment also regulated the expression of nerve growth factor and brain-derived neurotrophic factor in retina (Pagani et al., 2006), which may regulate retinal gene expression. During neural development, neural activities also regulate neuron gene expression and formation and mature of many synapses (Hensch, 2005; Hooks and Chen, 2006; Shah and Crair, 2008; Hong and Chen, 2011; Furman and Crair, 2012; Ackman and Crair, 2014). Therefore, mechanical stimulation at GB20 may activate and transfer neural signals into the brain and then control the retinal gene express by the feedback neural signal from the brain.

DATA AVAILABILITY STATEMENT

The datasets presented in this study can be found in online repositories. The names of the repository/repositories and accession number(s) can be found below: <https://www.ncbi.nlm.nih.gov/geo/>, GSE148759/b.

ETHICS STATEMENT

The animal study was reviewed and approved by the Animal Care and Use Committee of Beijing Institute of Technology and Peking University.

AUTHOR CONTRIBUTIONS

LM designed the experiments. JC, LZ, XG, RZ, YH, and QL performed the experiments and collected the data. LM and XL analyzed the data. HF drew the schematic image. LM prepared the figures and manuscript. All authors contributed to the article and approved the submitted version.

FUNDING

This work was supported by the National Natural Science Foundation of China (NSFC; 81803856). Portions of this work were supported by Beijing Institute of Technology Research Fund Program for Young Scholars.

ACKNOWLEDGMENTS

We thank the National Center for Protein Sciences at Peking University for assistance with imaging experiments.

REFERENCES

- Ackman, J. B., and Crair, M. C. (2014). Role of emergent neural activity in visual map development. *Curr. Opin. Neurobiol.* 24, 166–175. doi: 10.1016/j.conb.2013.11.011
- Bishop, P., Rocca, D., and Henley, J. M. (2016). Ubiquitin C-terminal hydrolase L1 (UCH-L1): structure, distribution and roles in brain function and dysfunction. *Biochem. J.* 473, 2453–2462. doi: 10.1042/bcj20160082
- Brusaferri, F., and Candelise, L. (2000). Steroids for multiple sclerosis and optic neuritis: a meta-analysis of randomized controlled clinical trials. *J. Neurol.* 247, 435–442. doi: 10.1007/s004150070172
- Chen, J., Zhang, L., Liu, L., Yang, X., Wu, F., Gan, X., et al. (2019). Acupuncture treatment reverses retinal gene expression induced by optic nerve injury via RNA sequencing analysis. *Front. Integr. Neurosci.* 13:59. doi: 10.3389/fnint.2019.00059
- de Seze, J. (2013). Inflammatory optic neuritis: from multiple sclerosis to neuromyelitis optica. *Neuroophthalmology* 37, 141–145. doi: 10.3109/01658107.2013.804232
- Deslauriers, A. M., Afkhami-Goli, A., Paul, A. M., Bhat, R. K., Acharjee, S., Ellestad, K. K., et al. (2011). Neuroinflammation and endoplasmic reticulum stress are coregulated by crocin to prevent demyelination and neurodegeneration. *J. Immunol.* 187, 4788–4799. doi: 10.4049/jimmunol.1004111
- Dietrich, M., Helling, N., Hilla, A., Heskamp, A., Issberner, A., Hildebrandt, T., et al. (2018). Early α -lipoic acid therapy protects from degeneration of the inner retinal layers and vision loss in an experimental autoimmune encephalomyelitis-optic neuritis model. *J. Neuroinflammation* 15:71. doi: 10.1186/s12974-018-1111-y
- Dobson, R., and Giovannoni, G. (2019). Multiple sclerosis—a review. *Eur. J. Neurol.* 26, 27–40. doi: 10.1111/ene.13819
- Dykes, I. M., Lanier, J., Eng, S. R., and Turner, E. E. (2010). Brn3a regulates neuronal subtype specification in the trigeminal ganglion by promoting Runx expression during sensory differentiation. *Neural Dev.* 5:3. doi: 10.1186/1749-8104-5-3
- Fernandes, K. A., Harder, J. M., Kim, J., and Libby, R. T. (2013). JUN regulates early transcriptional responses to axonal injury in retinal ganglion cells. *Exp. Eye Res.* 112, 106–117. doi: 10.1016/j.exer.2013.04.021

SUPPLEMENTARY MATERIAL

The Supplementary Material for this article can be found online at: <https://www.frontiersin.org/articles/10.3389/fnint.2020.568449/full#supplementary-material>.

FIGURE S1 | KEGG pathways analysis of DEGs induced by ON. **(A)** Bar plot lists the top enriched pathways based on *p*_{adj} value. **(B)** Dot plot shows the top enriched pathways based on DEG numbers. *p*_{adj}: adjusted *p*-value.

FIGURE S2 | Gene ontology enrichment analysis of needling treatments at GV16. **(A)** Bar plot lists the top 10 enrichments of each category based on *p*_{adj} value; yellow color highlights the top 3 of the most significantly enriched gene categories based on *p*_{adj} value. **(B)** Dot plot shows the top enriched gene categories based on DEG numbers; yellow highlights the top 3 of the enriched gene categories with most DEG numbers. BP, Biological Process; CC, Cellular Component; MF, Molecular Function. *p*_{adj}: adjusted *p*-value.

FIGURE S3 | Differentially expressed retinal genes after needling treatments at GB20 and GV16 in ON mice. **(A,B)** The volcano map shows the numbers of DEGs of retina after needling treatments at GB20 and GV16, respectively, compared with MOG immunization alone. *p*_{adj}: adjusted *p*-value.

TABLE S1 | Average FPKM values of differential expressed genes of all groups.

TABLE S2 | Average FPKM values of DEGs of GB20 group compared with MOG group.

TABLE S3 | Average FPKM values of DEGs of GV16 group compared with MOG group.

- Furman, M., and Crair, M. C. (2012). Synapse maturation is enhanced in the binocular region of the retinocollicular map prior to eye opening. *J. Neurophysiol.* 107, 3200–3216. doi: 10.1152/jn.00943.2011
- Gao, N., Liu, X., Wu, J., Li, J., Dong, C., Wu, X., et al. (2017). CXCL10 suppression of hem- and lymph-angiogenesis in inflamed corneas through MMP13. *Angiogenesis* 20, 505–518. doi: 10.1007/s10456-017-9561-x
- Gran, B., Zhang, G. X., Yu, S., Li, J., Chen, X. H., Ventura, E. S., et al. (2002). IL-12p35-deficient mice are susceptible to experimental autoimmune encephalomyelitis: evidence for redundancy in the IL-12 system in the induction of central nervous system autoimmune demyelination. *J. Immunol.* 169, 7104–7110. doi: 10.4049/jimmunol.169.12.7104
- Guo, B. J., Yu, S. Y., Shen, Z. F., and Hu, Y. P. (2017). Effect of acupuncture at points in heel vessel for circadian clock genes of period 1 and period 2 mRNAs in the suprachiasmatic nucleus in insomnia rats. *Zhen Ci Yan Jiu* 42, 507–509. doi: 10.13702/j.1000-0607.2017.06.007
- Hensch, T. K. (2005). Critical period plasticity in local cortical circuits. *Nat. Rev. Neurosci.* 6, 877–888. doi: 10.1038/nrn1787
- Hong, Y. K., and Chen, C. (2011). Wiring and rewiring of the retinogeniculate synapse. *Curr. Opin. Neurobiol.* 21, 228–237. doi: 10.1016/j.conb.2011.02.007
- Hooks, B. M., and Chen, C. (2006). Distinct roles for spontaneous and visual activity in remodeling of the retinogeniculate synapse. *Neuron* 52, 281–291. doi: 10.1016/j.neuron.2006.07.007
- Hou, S., Zheng, S., Chen, X., Wang, J. N., Zhong, Z. L., Chen, S. S., et al. (2018). Electroacupuncture intervention regulates circadian rhythms by down-regulating per gene expression in hypothalamic suprachiasmatic nucleus of hepatocellular carcinoma mice. *Zhen Ci Yan Jiu* 43, 632–639. doi: 10.13702/j.1000-0607.170678
- Huang, R., Chen, M., Yang, L., Wagle, M., Guo, S., and Hu, B. (2017). MicroRNA-133b negatively regulates zebrafish single mauthner-cell axon regeneration through targeting *tppp3* in vivo. *Front Mol Neurosci.* 10:375. doi: 10.3389/fnmol.2017.00375
- Huang, H., Miao, L., Liang, F., Liu, X., Xu, L., Teng, X., et al. (2017). Neuroprotection by eIF2 α -CHOP inhibition and XBP-1 activation in EAE/optic neuritis. *Cell Death Dis.* 8:e2936. doi: 10.1038/cddis.2017.329
- Hudson, C. D., Sayan, A. E., Melino, G., Knight, R. A., Latchman, D. S., and Budhram-Mahadeo, V. (2008). Brn-3a/POU4F1 interacts with and

- differentially affects p73-mediated transcription. *Cell Death Differ.* 15, 1266–1278. doi: 10.1038/cdd.2008.45
- Jenkins, T. M., and Toosy, A. T. (2017). Optic neuritis: the eye as a window to the brain. *Curr. Opin. Neurol.* 30, 61–66. doi: 10.1097/WCO.0000000000000414
- Jiao, N. J. (2011). Observation on therapeutic effect of age-related macular degeneration treated with acupuncture. *Zhongguo Zhen Jiu* 31, 43–45. doi: 10.13703/j.0255-2930.2011.01.013.
- Kemenyova, P., Turcani, P., Sutovsky, S., and Waczulikova, I. (2014). Optical coherence tomography and its use in optical neuritis and multiple sclerosis. *Bratisl. Lek. Listy* 115, 723–729. doi: 10.4149/bll_2014_140
- Kim, H. M., Cho, S. Y., Park, S. U., Sohn, I. S., Jung, W. S., Moon, S. K., et al. (2012). Can acupuncture affect the circadian rhythm of blood pressure? A randomized, double-blind, controlled trial. *J. Altern. Complement. Med.* 18, 918–923. doi: 10.1089/acm.2011.0508
- Kiryu-Seo, S., Sasaki, M., Yokohama, H., Nakagomi, S., Hirayama, T., Aoki, S., et al. (2000). Damage-induced neuronal endopeptidase (DINE) is a unique metalloproteinase expressed in response to neuronal damage and activates superoxide scavengers. *Proc. Natl. Acad. Sci. U S A* 97, 4345–4350. doi: 10.1073/pnas.070509897
- Kristiansen, H., Gad, H. H., Eskildsen-Larsen, S., Despres, P., and Hartmann, R. (2011). The oligoadenylate synthetase family: an ancient protein family with multiple antiviral activities. *J. Interferon. Cytokine. Res.* 31, 41–47. doi: 10.1089/jir.2010.0107
- Kumar, V., Mesentier-Louro, L. A., Oh, A. J., Heng, K., Shariati, M. A., Huang, H., et al. (2019). Increased ER stress after experimental ischemic optic neuropathy and improved RGC and oligodendrocyte survival after treatment with chemical chaperon. *Invest. Ophthalmol. Vis. Sci.* 60, 1953–1966. doi: 10.1167/iovs.18-24890
- Lassmann, H. (2018). Pathogenic mechanisms associated with different clinical courses of multiple sclerosis. *Front. Immunol.* 9:3116. doi: 10.3389/fimmu.2018.03116
- Lassmann, H. (2019). The changing concepts in the neuropathology of acquired demyelinating central nervous system disorders. *Curr. Opin. Neurol.* 32, 313–319. doi: 10.1097/wco.0000000000000685
- Lassmann, H., and Bradl, M. (2017). Multiple sclerosis: experimental models and reality. *Acta Neuropathol.* 133, 223–244. doi: 10.1007/s00401-016-1631-4
- Law, S. K., and Li, T. (2013). Acupuncture for glaucoma. *Cochrane Database Syst. Rev.* 5:CD006030. doi: 10.1002/14651858.cd006030
- Lei, Y., Jin, J., Ban, H., and Du, Y. (2017). Effects of acupuncture on circadian rhythm of blood pressure in patients with essential hypertension. *Zhongguo Zhen Jiu* 37, 1157–1161. doi: 10.13703/j.0255-2930.2017.11.005
- Li, Z., Chen, J., Cheng, J., Huang, S., Hu, Y., Wu, Y., et al. (2018). Acupuncture modulates the cerebello-thalamo-cortical circuit and cognitive brain regions in patients of Parkinson's disease with tremor. *Front. Aging Neurosci.* 10:206. doi: 10.3389/fnagi.2018.00206
- Locri, F., Cammalleri, M., Pini, A., Dal Monte, M., Rusciano, D., and Bagnoli, P. (2018). Further evidence on efficacy of diet supplementation with fatty acids in ocular pathologies: insights from the EAE model of optic neuritis. *Nutrients* 10:1447. doi: 10.3390/nu10101447
- Miyachi, S., Gopal, E., Fei, Y. J., and Ganapathy, V. (2004). Functional identification of SLC5A8, a tumor suppressor down-regulated in colon cancer, as a Na⁺-coupled transporter for short-chain fatty acids. *J. Biol. Chem.* 279, 13293–13296. doi: 10.1074/jbc.c400059200
- Nashine, S., Liu, Y., Kim, B. J., Clark, A. F., and Pang, I. H. (2014). Role of C/EBP homologous protein in retinal ganglion cell death after ischemia/reperfusion injury. *Invest. Ophthalmol. Vis. Sci.* 55, 221–231. doi: 10.1167/iovs.14-15447
- Oakes, S. R., Gallego-Ortega, D., Stanford, P. M., Junankar, S., Au, W. W. Y., Kikhtyak, Z., et al. (2017). A mutation in the viral sensor 2'-5'-oligoadenylate synthetase 2 causes failure of lactation. *PLoS Genet.* 13:e1007072. doi: 10.1371/journal.pgen.1007072
- Pagani, L., Manni, L., and Aloe, L. (2006). Effects of electroacupuncture on retinal nerve growth factor and brain-derived neurotrophic factor expression in a rat model of retinitis pigmentosa. *Brain Res.* 1092, 198–206. doi: 10.1016/j.brainres.2006.03.074
- Pak, W., Hindges, R., Lim, Y. S., Pfaff, S. L., and O'Leary, D. D. (2004). Magnitude of binocular vision controlled by islet-2 repression of a genetic program that specifies laterality of retinal axon pathfinding. *Cell* 119, 567–578. doi: 10.1016/j.cell.2004.10.026
- Pönniö, T., and Conneely, O. M. (2004). nor-1 regulates hippocampal axon guidance, pyramidal cell survival and seizure susceptibility. *Mol. Cell. Biol.* 24, 9070–9078. doi: 10.1128/mcb.24.20.9070-9078.2004
- Qin, Y., Yuan, W., Deng, H., Xiang, Z., Yang, C., Kou, X., et al. (2015). Clinical efficacy observation of acupuncture treatment for nonarteritic anterior ischemic optic neuropathy. *Evid. Based Complement. Alternat. Med.* 2015:713218. doi: 10.1155/2015/713218
- Quinn, T. A., Dutt, M., and Shindler, K. S. (2011). Optic neuritis and retinal ganglion cell loss in a chronic murine model of multiple sclerosis. *Front. Neurol.* 2:50. doi: 10.3389/fneur.2011.00050
- Rappert, A., Bechmann, I., Pivneva, T., Mahlo, J., Biber, K., Nolte, C., et al. (2004). CXCR3-dependent microglial recruitment is essential for dendrite loss after brain lesion. *J. Neurosci.* 24, 8500–8509. doi: 10.1523/jneurosci.2451-04.2004
- Reich, D. S., Lucchinetti, C. F., and Calabresi, P. A. (2018). Multiple sclerosis. *N. Engl. J. Med.* 378, 169–180. doi: 10.1056/NEJMra1401483
- Shah, R. D., and Crair, M. C. (2008). Retinocollicular synapse maturation and plasticity are regulated by correlated retinal waves. *J. Neurosci.* 28, 292–303. doi: 10.1523/jneurosci.4276-07.2008
- Soto, I., Oglesby, E., Buckingham, B. P., Son, J. L., Roberson, E. D., Steele, M. R., et al. (2008). Retinal ganglion cells downregulate gene expression and lose their axons within the optic nerve head in a mouse glaucoma model. *J. Neurosci.* 28, 548–561. doi: 10.1523/jneurosci.3714-07.2008
- Stevanato, L., and Sinden, J. D. (2014). The effects of microRNAs on human neural stem cell differentiation in two- and three-dimensional cultures. *Stem Cell Res. Ther.* 5:49. doi: 10.1186/scrt437
- Stone, S., and Lin, W. (2015). The unfolded protein response in multiple sclerosis. *Front. Neurosci.* 9:264. doi: 10.3389/fnins.2015.00264
- Torre-Fuentes, L., Moreno-Jimenez, L., Pytel, V., Matias-Guiu, J. A., Gomez-Pinedo, U., and Matias-Guiu, J. (2020). Experimental models of demyelination and remyelination. *Neurologia* 35, 32–39. doi: 10.1016/j.nrl.2017.07.002
- Volakakis, N., Kadkhodaei, B., Joodmardi, E., Wallis, K., Panman, L., Silvaggi, J., et al. (2010). NR4A orphan nuclear receptors as mediators of CREB-dependent neuroprotection. *Proc. Natl. Acad. Sci. U S A* 107, 12317–12322. doi: 10.1073/pnas.1007088107
- Wei, X. R., Wei, G. W., Zheng, X. N., Wu, X. F., Chen, X. L., Liu, L., et al. (2017). Effect of acupuncture stimulation of different acupoint combinations on sleep and expression of circadian clock and Bmal 1 genes in hypothalamus of insomnia rats. *Zhen Ci Yan Jiu* 42, 429–433. doi: 10.13702/j.1000-0607.2017.05.010
- Woung, L. C., Chung, H. C., Jou, J. R., Wang, K. C., and Peng, P. H. (2011). A comparison of optic neuritis in Asian and in Western Countries. *Neuroophthalmology* 35, 65–72. doi: 10.3109/01658107.2011.557851
- Xu, J., and Peng, Q. (2015). Retinitis pigmentosa treatment with western medicine and traditional chinese medicine therapies. *J. Ophthalmol.* 2015:421269. doi: 10.1155/2015/421269
- Xu, H., Wang, S., and Guo, M. H. (2012). ZHANG Ren's experience of treatment on glaucoma with acupuncture. *Zhongguo Zhen Jiu* 32, 444–447. doi: 10.13703/j.0255-2930.2012.05.020
- Yang, M., Yu, Z., Deng, S., Chen, X., Chen, L., Guo, Z., et al. (2016). A targeted metabolomics MRM-MS study on identifying potential hypertension biomarkers in human plasma and evaluating acupuncture effects. *Sci. Rep.* 6:25871. doi: 10.1038/srep25871
- Yue, Y., Stanojlovic, M., Lin, Y., Karsenty, G., and Lin, W. (2019). Oligodendrocyte-specific ATF4 inactivation does not influence the development of EAE. *J. Neuroinflammation* 16:23. doi: 10.1186/s12974-019-1415-6

Conflict of Interest: The authors declare that the research was conducted in the absence of any commercial or financial relationships that could be construed as a potential conflict of interest.

Copyright © 2020 Chen, Zhang, Gan, Zhang, He, Lv, Fu, Liu and Miao. This is an open-access article distributed under the terms of the Creative Commons Attribution License (CC BY). The use, distribution or reproduction in other forums is permitted, provided the original author(s) and the copyright owner(s) are credited and that the original publication in this journal is cited, in accordance with accepted academic practice. No use, distribution or reproduction is permitted which does not comply with these terms